11892 *Biochemistry* **2009,** *48,* 11892–11901
DOI: 10.1021/bi901668y

BIOCHEMISTRY
including biophysical chemistry & molecular biology
Article

Solution Structure and Membrane Interactions of the Antimicrobial Peptide Fallaxidin 4.1a: An NMR and QCM Study[†]

Patrick J. Sherman,[‡] Rebecca J. Jackway,[‡] John D. Gehman,[§] Slavica Praporski,[#] George A. McCubbin,[#] Adam Mechler,[#] Lisandra L. Martin,[#] Frances Separovic,*[,§] and John H. Bowie[‡]

[‡]*Department of Chemistry, The University of Adelaide, South Australia 5005, Australia,* [§]*School of Chemistry, Bio21 Institute, University of Melbourne, Victoria 3010, Australia, and* [#]*School of Chemistry, Monash University, Victoria 3800, Australia*

Received September 24, 2009; Revised Manuscript Received November 5, 2009

ABSTRACT: The solution structure of fallaxidin 4.1a, a C-terminal amidated analogue of fallaxidin 4.1, a cationic antimicrobial peptide isolated from the amphibian *Litoria fallax*, has been determined by nuclear magnetic resonance (NMR). In zwitterionic dodecylphosphocholine (DPC) micelles, fallaxidin 4.1a adopted a partially helical structure with random coil characteristics. The flexibility of the structure may enhance the binding and penetration upon interaction with microbial membranes. Solid-state ^{31}P and ^{2}H NMR was used to investigate the effects of fallaxidin 4.1a on the dynamics of phospholipid membranes, using acyl chain deuterated zwitterionic dimyristoylphosphatidylcholine (DMPC-d_{54}) and anionic dimyristoylphosphatidylglycerol (DMPG) multilamellar vesicles. In DMPC-d_{54} vesicle bilayers, fallaxidin 4.1a caused a decrease in the ^{31}P chemical shift anisotropy (CSA), and a decrease in deuterium order parameters from the upper acyl chain region, indicating increased lipid motion about the phosphate headgroups. Conversely, for DMPC-d_{54}/DMPG, two ^{31}P CSA were observed due to a lateral phase separation of the two lipids and/or differing headgroup orientations in the presence of fallaxidin 4.1a, with a preferential interaction with DMPG. Little effect on the deuterated acyl chain order parameters was observed in the d_{54}-DMPC/DMPG model membranes. Real time quartz crystal microbalance analyses of fallaxidin 4.1a addition to DMPC and DMPC/DMPG supported lipid bilayers together with the NMR results indicated transmembrane pore formation in DMPC/DMPG membranes and peptide insertion followed by disruption at a threshold concentration in DMPC membranes. The different interactions observed with "mammalian" (DMPC) and "bacterial" (DMPC/DMPG) model membranes imply fallaxidin 4.1a may be a useful antimicrobial peptide, with preferential cytolytic activity toward prokaryotic organisms at low peptide concentrations ($< 5\ \mu$M).

Amphibians live in environments that are rich in microbial flora, against which they require an adequate defense immune mechanism (*1*). Antimicrobial peptides form an important front-line defense against invading microbes (*2*). Generally, amphibian species produce a unique collection of antimicrobial peptides that significantly vary in length, hydrophobicity, and charge. While the antimicrobial action of these peptides is to some extent a result of their synergistic effects, single, isolated peptides have also been noted to have a spectrum of activity that reaches beyond bacterial targets to include fungal and eukaryotic cells. An amphibian peptide, temporin A, has also been shown to indirectly affect antimicrobial activity by acting as an intracellular signal to coordinate the innate and adaptive host defense to initiate processes such as wound healing, angiogenesis, and cell proliferation (*3*).

Traditional antibiotic therapeutic agents target the enzymes and receptors that form integral components of the bacterial biochemistry. Rapid adaptation by bacteria has led to the appearance of numerous drug-resistant bacteria strains (*4*, *5*). Antimicrobial peptides on the other hand act via a nonreceptor mediated method that results in the disruption of the target membrane (*6*−*10*). In nature, the diversity of peptides simultaneously secreted by amphibians is likely designed to counter the diversity of potentially infectious bacteria and resistance is, therefore, unlikely. Amphibian peptides, consequently, provide several attractive leads for therapeutic prospects in modern medicine (*11*). The mechanisms of action and the factors that govern their selectivity must be understood, however, before the task of developing nonhydrolyzable analogues can begin.

Amphibians produce around 20% of the known antimicrobial peptides. Typically, these peptides are 11−46 residues long (*12*), positively charged due to the high content of Lys and Arg residues, and are encoded by genes displaying high homology between species (*13*). These antimicrobial peptides are generally classified into two broad classes based on their chemical structure: linear, largely α-helical peptides, and peptides held in *β*-sheet conformations via cystine linkages (*13*, *14*). A common characteristic of linear antimicrobial peptides is the propensity to form amphipathic α-helices. The positively charged regions of the helix bind to the negatively charged lipid bilayers of bacterial membranes, thereby disrupting them. Interestingly, antimicrobial peptides display activity against a broad spectrum of microorganisms including bacteria, fungi, viruses, and malaria parasites (*12*), in addition to antitumor activity (*15*).

These amphipathic α-helical peptides interact with and disturb the function of bacterial membranes by mechanisms as described by two models, the "carpet" (*16*) and the "barrel-stave" mechanisms (*7*). In the carpet model, the peptides assemble parallel to the membrane surface, acting in a detergent-like manner that strains the bilayer and results in the formation of transient defects or

[†]Grant sponsor: Australian Research Council.
*To whom correspondence should be addressed. Phone: +61 3 8344 2447; fax: +61 3 9347 5180; e-mail: fs@unimelb.edu.au.

 Published on Web 11/07/2009

pores. The membrane may ultimately break up into small vesicles coated by the peptide (*17*). Alternatively, for the barrel-stave model the peptides insert themselves into the membrane and aggregate, forming transmembrane pores that disrupt the osmotic potential of the cell (*7*, *18*). Another transmembrane model is the "toroidal" pore, where both the peptides and the lipid headgroups line the lumen of the pore (*19*). A minimum of 20 residues is required to span the membrane as an α-helix, although for smaller peptides a modified model has been proposed whereby these peptides dimerize end-to-end to effect complete penetration (*19*, *20*). In both surface and transmembrane models, the disruption of the membrane leads to the breakdown of the transmembrane potential and ion gradients, creating leakage of the cellular contents resulting in cell death.

Australian amphibians have proved to be an abundant source of antimicrobial peptides including the aureins (*21*), citropins 1 (*22*), caerins 1 (*23*, *24*), dahleins 1 (*25*), uperins (*26*), and maculatins (*27*, *28*), many of which are small cationic peptides that adopt amphipathic α-helical structures in lipid environments. In addition to their antimicrobial activities, many of these peptide types show fungicide activity against chytrid fungus (*Batrachochytrium dendrobatidis*), which is widespread among Australian anuran species (*15*). The caerin peptides, for instance, have C-terminal amides and basic residues concentrated in the C-terminal region. Caerin 1.1, which has been studied extensively, adopts a helix−hinge−helix conformer (*29*) and appears to disrupt model membranes via a transmembrane interaction (*30*). Caerin 1.1 is a wide spectrum antimicrobial agent against Gram-positive bacteria but has also been shown to be an anticancer agent against most types of human tumors and active against enveloped viruses including HIV and *Herpes simplex 1* (*31*) at much lower concentrations than that which is toxic to cells (*12*). It also is an antifungal agent, kills nematodes, and inhibits the formation of NO by nNOS (*15*).

As part of our ongoing studies of the host defense peptides contained in the glandular secretions of Australian anurans [for reviews see refs *15* and *31*], we have recently studied the skin peptides of the Eastern Dwarf Tree Frog *Litoria fallax* (*32*). Of the peptides isolated from *L. fallax*, one peptide, fallaxidin 4.1 displays modest antimicrobial activity. The sequence of fallaxidin 4.1 is unusual, in that it contains three Pro residues and has a C-terminal free carboxylic acid group, features not typically present in antimicrobial peptides (*33*, *34*). We have found that adding the C-terminal amide considerably increases the activity of fallaxidin 4.1 against several Gram-positive bacteria (Table 1). Consequently, we now report the solution structures of fallaxidin 4.1 and its amidated analogue fallaxidin 4.1a in a membrane-like environment using solution state NMR[1] spectroscopy and computational calculations.

Although the solution structure of the peptide is important for assisting in understanding its antimicrobial activity, it is also essential to investigate the perturbations of membrane bilayers by the peptide. Solid-state NMR spectroscopy has been widely used for this purpose and applied to model lipid membranes (*35*−*37*). The lipids investigated have naturally abundant ^{31}P in the phospholipid headgroup and synthetically incorporated ^{2}H in the acyl chains. This allows the order and dynamics of the lipid molecules to be probed over a wide range of time scales (*35*, *38*−*42*). In addition, real time analysis of peptide interactions upon addition to lipid bilayers is observed using quartz crystal microbalance (QCM), by monitoring the change in frequency (Δf) and dissipation (ΔD) of a resonating quartz chip coated with a supported lipid bilayer (*43*−*45*). QCM probes the immediate interaction between the peptide and the membrane prior to an equilibrium state, thereby enabling some elucidation of the pathway. Consequently, solid-state NMR spectroscopy and QCM are complementary techniques for studying the mechanism of interaction of the peptide with the lipid membrane.

The aims of this study are 3-fold: (i) to investigate the influence of the C-terminal group on the antimicrobial activity of fallaxidin 4.1, (ii) to determine the solution structure of fallaxidin 4.1 and its amide analogue (fallaxidin 4.1a) in membrane environments and provide insight into their conformations when associated with a lipid membrane, and (iii) to obtain information about the interactions of the most active analogue with biomimetic membranes. The results presented here provide some insight into the mechanism by which fallaxidins 4.1 and 4.1a exert their antimicrobial activities.

Table 1: Antimicrobial Data for Fallaxidin 4.1 and its C-Terminal Amide Analogue Fallaxidin 4.1a [MIC ($\mu g \cdot mL^{-1}$)][a]

fallaxidin 4.1	GLLSF LPKVI GVIGH LIHPP S−OH
fallaxidin 4.1a	GLLSF LPKVI GVIGH LIHPP S-NH_2

bacteria[b]	fallaxidin 4.1	4.1a
Gram Positive		
Bacillus cereus[c]	−[b]	25
Enterococcus faecalis (ATCC29212)	−[b]	50
Leuconostoc lactis[c]	12	3
Listeria innocua[c]	−[b]	50
Micrococcys luteus (ATCC9341)	100	12
Staphylococcus aureus (ATCC29213)	−[b]	25
Staphylococcus epidermidis (ATCC14990)	100	25
Streptococcus uberis[c]	50	12
Gram Negative		
Enterobacter cloacae (ATCC13047)	−[b]	−[b]
Escherichia coli (ATCC35218)	−[b]	−[b]

[a]MIC − minimum inhibitory concentration that inhibits the visible growth of a microbe. [b]Indicates that there is no activity ≤100 $\mu g \cdot mL^{-1}$. [c]Wild strain.

MATERIAL AND METHODS

Solution-State NMR Spectroscopy. Fallaxidin 4.1 and its amide modification were synthesized with L-amino acids

[1]Abbreviations: 2D, two-dimensional; CSA, chemical shift anisotropy; DQF-COSY, double quantum filtered correlation spectroscopy; DMPC, dimyristoylphosphatidylcholine; DMPG, dimyristoylphosphatidylglycerol; DPC, dodecylphosphocholine; DSS, 4,4-dimethyl-4-silapentane-1-sulfonic acid; ESI-MS, electrospray ionization mass spectrometry; FID, free induction decay; HPLC, high performance liquid chromatography; HSQC, heteronuclear single quantum coherence; MIC, minimum inhibitory concentration; MLV, multilamellar vesicles; MOPS, 3-(*N*-morpholino) propanesulfonic acid; MPA, 3-mercaptopropionic acid; NMR, nuclear magnetic resonance; NOE, nuclear Overhauser effect; NOESY, nuclear Overhauser effect spectroscopy; QCM, quartz crystal microbalance; RMD, restricted molecular dynamic; SA, simulated annealing; TFE, 2,2,2-trifluoroethanol.

using the standard N-α-Fmoc method, by GenScript Corp (Piscataway, NJ) (*46*) and shown to be of greater than 95% purity, determined by HPLC and ESI-MS. Solution studies were carried out in trifluoroethanol (TFE)/water and in aqueous dodecylphosphocholine (DPC) micelles by codissolving the fallaxidin 4.1a (7.67 mg, 3.5 μmol) and 40 mol equiv of DPC (54.56 mg, 140 μmol) in an aqueous solution containing 10% D_2O and 50 mM NaH_2PO_4 buffer to produce a final volume of 0.7 mL. The pH was adjusted to 6.0 (using sodium hydroxide) and a single crystal of DSS was added as a chemical shift reference.

A Varian (Varian Inc., Palo Alto, CA) Inova-600 NMR spectrometer using a ^1H frequency of 600 MHz and a ^{13}C frequency of 150 MHz was used for acquisition of all NMR spectra. Experiments were run at 25 °C and ^1H NMR spectra were referenced to DSS (0.0 ppm).

High-resolution 1D ^1H NMR spectra were acquired for the fallaxidins 4.1 and 4.1a using 0.125 Hz per point digital resolution to obtain $^3J_{NH\text{-}\alpha H}$ coupling constants, which are used for backbone torsion angle restraints in structure calculations. 2D NMR experiments TOCSY, DQF-COSY, and NOESY were acquired in phase-sensitive mode, using time proportional phase incrementation in t_1 (*47*). Typically 64 time-averaged scans were acquired per increment, totalling 200 increments per experiment with spectral width of 6999.7 Hz. The FID in t_2 contained 2048 data points spread over a spectral width of 6999.7 Hz. A 90° pulse was calibrated for each experiment and a recycle delay of 1 s was incorporated. NOESY spectra were acquired using mixing times of 100 ms. TOCSY pulse sequences included a 60 ms spin-lock. Presaturation was used to suppress water resonances. The $^{13}C-^1H$ HSQC experiments were recorded with an interpulse delay of $1/2J_{CH} = 3.6$ ms corresponding to $J_{CH} = 140$ Hz. In the $^{13}C-^1H$ HSQC experiment 200 increments were used, each consisting of 64 scans. The FID in the directly detected ^1H, F_2 dimension consisted of 4096 data points and spectral width of 6999.7 Hz. A spectral width in the ^{13}C, F_1 dimension of 21114.5 Hz was also used.

2D NMR experiments were processed on a Sun Microsystems Ultra Sparc 1/170 workstation using VNMR software (VNMRJ, version 1.1D). Data matrices were multiplied by a Gaussian factor of 0.15 in the direct dimension and zero-filled to 2048 (for $^1H-^1H$ experiments) or 4096 (for $^{13}C-^1H$ HSQC) points in t_1 before Fourier transformation.

Structure Calculations. Cross-peaks in TOSCY and NOESY spectra were assigned using SPARKY software (version 3.106) and a standard sequential assignment method (*48*). The NOESY cross-peak volumes were converted to distance restraints as described by Xu (*49*). When symmetric pairs of cross-peaks were present, the larger peak volume was used and converted to a distance restraint (*50*). ^1H dihedral angles were restrained to $^3J_{NH\alpha H} < 5$ Hz, $\phi = -60° \pm 30°$ and $5 < {}^3J_{NH\alpha H} < 6$ Hz, $\phi = -60° \pm 40°$. For $^3J_{NH\alpha H} > 6$ Hz, ϕ angles were not restrained.

Structures were generated using ARIA (version 1.2) applied with CNS Solve (version 1.1). The standard RMD and SA method of ARIA was used (*51*) with the inclusion of floating stereospecific assignments to enable the assignment of distance restraints relating to methylene and isopropyl group resonances (*52*). Each ARIA run was comprised of eight iterations. Better convergence was achieved using parameters based on those previously used (*53*, *54*). 60 structures were calculated in the final iteration and the 20 lowest potential energy structures were selected for analysis. The final 3D structures was displayed using VMD software (version 1.8.2) (*55*) and MOLMOL (version 2k.2) (*56*).

Solid-State NMR Spectroscopy. Phospholipids, dimyristoylphosphatidylcholine (DMPC), deuterated DMPC (DMPC-d_{54}), and dimyristoylphosphatidylglycerol (DMPG), were obtained from Avanti Polar Lipids (Alabaster, AL) and used without further purification. Fallaxidin 4.1a (2.1 mg, 1 μmole) was codissolved with either a 1:1 molar mixture of DMPC-d_{54}/DMPC or a 1:1:1 molar mixture of DMPC-d_{54}/DMPC/DMPG using 1 mL of MeOH/$CHCl_3$ (1:1 v/v), producing a lipid/peptide ratio of 10:1. The organic solvent was removed via rotary evaporation (250 mbar, 30 °C) to form a thin lipid/peptide film in a round-bottom flask, and the samples lyophilized overnight. The dried samples were hydrated with 100 μL of 50 mM 3-(*N*-morpholino) propanesulfonic acid (MOPS) (150 mM NaCl, pH 7) buffer, subjected to five freeze−thaw/vortex cycles and centrifuged (1 min, 4000 rpm). The resultant viscous translucent suspensions were transferred to 5 mm NMR tubes for NMR analysis. The "neutral" DMPC and "anionic" DMPC/DMPG controls were prepared in a similar manner, without the addition of fallaxidin 4.1a.

All solid-state NMR experiments were performed on a Varian (Palo Alto, CA) Inova-300 spectrometer, using a 5 mm Doty (Columbia, SC) MAS probe at 30 °C. Static proton decoupled ^{31}P NMR spectra were obtained at an operating frequency of 121.5 MHz using a Hahn spin−echo pulse sequence with a 5.8 μs 90° pulse, 62 μs interpulse delay, and a 4 s recycle delay. ^{31}P NMR spectra were averaged over 60 000 scans at a spectral width of 125 kHz with 100 Hz exponential line broadening upon processing. Overlapped ^{31}P lineshapes were deconvoluted using the DMFIT program, employing the "CSA static" model (*57*) for a hydrated phospholipid bilayer (where CSA = $\sigma_\perp - \sigma_\parallel$) (*58*).

^2H NMR spectra were obtained at an operating frequency of 46.1 MHz using a quadrupolar-echo pulse sequence with a 3.8 μs 90° pulse, 40 μs interpulse delay, and a 0.5 s recycle delay. ^2H NMR spectra were averaged over 160 000 scans at a spectral width of 500 kHz with 100 Hz exponential line broadening. The overlapping Pake doublets from the unoriented deuterium spectra were "dePaked" using single value decomposition (*39*, *59*−*61*), numerical calculations were administered by GNU Scientific library v.1.11 (*62*) and graphical outputs generated with gnuplot v4.2.4 (*63*).

QCM of Fallaxidin 4.1a on Supported Phospholipid Bilayers. A quartz crystal microbalance (QCM) was used to examine the influence of fallaxidin 4.1a on supported phospholipid bilayers. QCM measurements were performed using the Q-Sense E4 system (Q-Sense, Sweden). The sensor crystals used were 5 MHz, AT-cut, quartz discs (chips) with an evaporated gold surface (Q-Sense). The resonance frequency and energy dissipation were measured simultaneously at the fundamental frequency of the crystal (1st harmonic at 5 MHz) and four harmonics of the fundamental frequency (third, fifth, seventh, and ninth harmonic at 15, 25, 35, and 45 MHz, respectively) (*45*). Raw data were analyzed by QTools (Q-Sense) and Origin 7.5 (OriginLab, Northampton, MA) software. The buffer used throughout the QCM experiments was phosphate buffered saline (PBS), containing 0.1 M NaCl and 20 mM phosphate (pH 6.9). Sodium chloride (Ultra, ≥ 99.5%), potassium phosphate monobasic, and potassium phosphate dibasic (ACS reagent, ≥ 99%) were purchased from Sigma-Aldrich (Castle Hill, Australia). All experiments were performed at 19.10 ± 0.05 °C.

Supported phospholipid bilayers were prepared using a liposome deposition procedure, whereby liposomes are allowed to spontaneously rupture and fuse together to form bilayers on a 3-mercaptopropionic acid (MPA) modified chip. Liposome solutions of either neat DMPC or DMPC/DMPG (2:1) composition were prepared as previously described (*43*). The liposome solutions (0.13 mM) were introduced into the QCM cells at a flow rate of 100 mL/min. Nonruptured liposomes were rinsed off with buffer. After a baseline had been established, the peptide solution (1, 2, 5, 7, 10, and 20 mM in buffer; total volume of 1 mL) was flowed through the cells at 100 mL/min. The peptide was left to incubate with the lipid bilayer for at least 20 min and then the cells were rinsed with buffer.

Chip Cleaning and Surface Modification. Before each experiment, the QCM chips were cleaned in a 1:1:3 mixture of ammonia (28%, Finechem, Seven Hills, Australia), hydrogen peroxide (30%, Merck, Kilsyth, Australia), and ultrapure water (18.2 MΩ·cm, Sartorius AG, Goettingen, Germany), at ca. 70 °C for 15−20 min. The chips were then thoroughly rinsed with ultrapure water and propane-2-ol (Merck, Kilsyth, Australia) prior to immersion into a 1 mM solution of MPA (≥99%, Fluka, Bio-Chimica, Switzerland) in propane-2-ol, for at least 30 min. The chips were subsequently rinsed with propane-2-ol, dried under a gentle stream of N_2 gas and assembled into the QCM cells ready for use.

Antibiotic Testing. Peptides were tested for antibiotic activity at varying concentrations by the Institute of Medical and Veterinary Science (Adelaide, Australia). The method used involved the measurement of inhibition zones on an agarose plate containing the microorganisms listed in Table 1 (*64*).

RESULTS

Synthetic Modification of Fallaxidin 4.1. Fallaxidin 4.1 shows modest antimicrobial activity against some of the Gram positive bacteria tested (Table 1) despite containing (i) three Pro residues, which must significantly reduce the helicity and amphipathicity of membrane-active antimicrobials, and (ii) the C-terminal free acid group, which reduces the overall positive charge of the peptide. In order to investigate the influence of the C-terminal acid group, we have studied the activity of a fallaxidin 4.1 synthetic modification where the C-terminal residue is amidated (fallaxidin 4.1a). The antimicrobial data recorded in Table 1 show fallaxidin 4.1a had an approximate 4-fold activity enhancement against microbes affected by fallaxidin 4.1 (MIC ≤ 100 $\mu g \cdot mL^{-1}$), and was active against all Gram positive bacteria tested. This enhanced activity of the amidated analogue illustrates the significance of the net positive charge of the peptide to antimicrobial activity.

Solution-State NMR Spectroscopy. The antimicrobial activity of fallaxidins 4.1 and 4.1a are unusual, as the peptide sequence with three proline residues is not consistent with those of other amphipathic membrane-active antimicrobial peptides isolated from tree frogs of the genus *Litoria* (*15*, *31*). We have investigated the 3D solution structure of the two peptides by 2D NMR in TFE/water (1:1 v/v), a reduced dielectric solvent system, which may mimic the membrane environment. The solution structures of fallaxidins 4.1 and 4.1a were essentially the same (apart from the C-terminal group) in aqueous TFE (*64*), and so we now concentrate on the solution structure of the more active amide analogue (fallaxidin 4.1a) in DPC micelles in order to investigate the solution structure at the site of action: the membrane.

NMR spectra were acquired for fallaxidin 4.1a in DPC micelles (40:1 lipid/peptide ratio) and the proton chemical shifts were assigned using a combination of NOESY, TOCSY, and COSY experiments and standard sequential assignment methods (*48*). αC resonances were assigned by investigation of the αH/αC region of a HSQC spectrum. A summary of the ^{1}H and αC ^{13}C resonances can be found in the Supporting Information, Table S1, and secondary chemical shifts (Supporting Information, Figure S1) along with partial NOESY, TOCSY, and HSQC spectra (Supporting Information, Figures S2 and S3).

There is a general upfield shift for the αH resonances from random coil values (*65*) for the N-terminal residues consistent with a helical structure, with some disruption to the helical shift from around Ile13 (Supporting Information, Figure S1a) and at the C-terminus. Although it was anticipated that there would be a lack of defined secondary structure at the ends of the peptide as a result of a reduction in hydrogen bonding (*66*), there appeared to be a trend toward random coil values observed for the residues C-terminal to Ile13, which suggests that this region of the peptide is unstructured. The αC secondary shifts (Supporting Information, Figure S1b) further support this, illustrating two distinct regions: a helical region from Ser4 to Ile13 as indicated by the

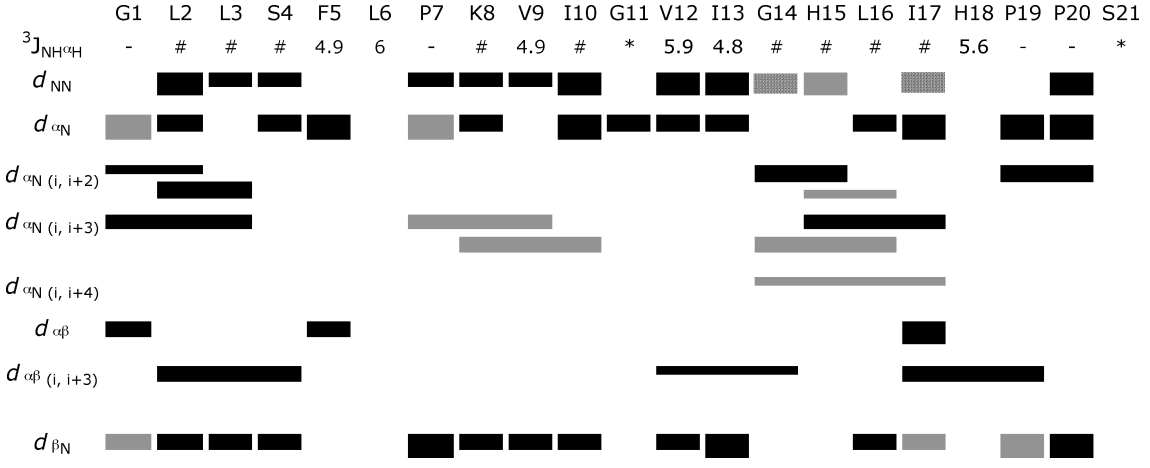

FIGURE 1: A summary of the diagnostic NOE connectivities used in the structure calculations for fallaxidin 4.1a in DPC micelles. The thickness of the bar indicates the relative strength of the NOEs (strong < 3.1 Å, medium 3.1−3.7 Å, weak > 3.7 Å). Gray shaded bars represent ambiguous NOEs. For Pro where no amide proton is present, NOEs to δH are shown. $^3J_{NH\alpha H}$ values are indicated where applicable. # indicates coupling constants that were not resolved due to signal overlap, * indicates no coupling constant was detected.

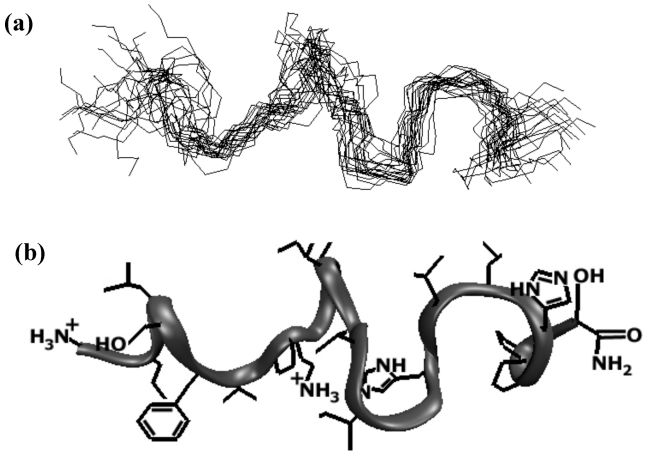

FIGURE 2: (a) The 20 lowest potential energy calculated structures of fallaxidin 4.1a in DPC micelles. The structures have been aligned over the backbone atoms. (b) The most stable calculated structure of fallaxidin 4.1a in DPC micelles.

downfield shift from the random coil values (*67*), and a region with less defined structure (Ile13 to Ser21) as indicated by the near zero secondary shifts. The NH secondary shift values deviate periodically over three to four residues, with the resonances of the hydrophilic residues generally upfield relative to those of the hydrophobic residues (Supporting Information, Figure S1c), which is common in α-helical structures (*67*). The exception to this is in the vicinity of Ile13 (Gly11 to His15), suggesting that this region of the peptide does not display defined amphipathicity.

A summary of the diagnostic NOE connectivities for fallaxidin 4.1a in DPC micelles is shown in Figure 1. Strong sequential d_{NN}, $d_{\alpha N}$, and $d_{\beta N}$ NOEs were observed along most of the sequence. A number of medium range NOE connectivities was observed from three residues apart, notably $d_{\alpha N(i,i+3)}$ and $d_{\alpha\beta(i,i+3)}$ signals. The absence of medium range NOEs at the C-terminus from His18 and in the regions of Ser4 to Leu6 and Gly11 to Ile13 suggests that in these regions, some disruption to the defined secondary structure is present. The remaining regions of the peptide had NOE connectivity patterns consistent with helical secondary structure (*48*). No long-range NOEs were observed, signifying a lack of intermolecular association.

The extent of *cis*−*trans* isomerization of the Pro residues can be determined from the observed NOEs about the Pro imide bond (*68*). As $d_{\alpha\delta}$ and not $d_{\alpha\alpha}$ signals were present, it is likely that the *trans* isomer is the dominant isomer for all of the three Pro residues.

A total of 275 nonredundant distance restraints were generated from the NOESY spectrum, including 44 ambiguous restraints, which were used for the structure calculations. The energy and statistics for the generated structures of fallaxidin 4.1a in DPC micelles can be found in the Supporting Information (Table S2). The average backbone torsion angles are also shown in a Ramachandran plot (Supporting Information, Figure S3). Several dihedral restraints derived from the $^3J_{NH\alpha H}$ coupling constants (Figure 1) were also employed in the structure calculations. The values of these coupling constants were consistent with regions of helical secondary structure.

The 20 lowest energy structures of fallaxidin 4.1a aligned over the backbone atoms are shown in Figure 2a. The helicity in the C-terminus appears to be inconsistent with the chemical shift data (Supporting Information, Figure S1) and may be due to conformational averaging due to peptide dynamics, with the NOESY data giving a time averaged distance (*67*). The most energetically stable calculated structure is shown in Figure 2b. Fallaxidin 4.1a displays regions of defined secondary structure resembling an α-helix. However, structure disruptions by Gly11 and Gly14 result in the central region of the peptide between these two residues displaying a more extended strand-like structure. Further disruption to the helical structure is observed at Pro7. Overall, the secondary structure of fallaxidin 4.1a appears to be helical with a disruption to this structure in the region of Pro7, Gly11, and Gly14.

Solid-State NMR Spectroscopy. Solid-state ^{31}P NMR has been employed to detect alterations in the dynamics and orientations of polar head groups of phospholipids. The line shape or chemical shift anisotropy (CSA) of the static ^{31}P spectra gives an indication of the motion and alignment of the phosphate head groups due to changes in orientation and surface charge density (*58*, *69*, *10*). The unoriented lineshapes showed axially symmetric CSA properties, which indicate the lipids are in the fluid or lamellar (L_α) phase (*69*). The overlapping ^{2}H quadrupolar spittings from the static ^{2}H NMR spectra (*70*−*72*) were "dePaked" to further calculate the order parameters (S_{CD}) of the DMPC (Table S3, Figure 5), which indicate the degree of disorder of the CD_2/CD_3 groups of the deuterated phospholipid acyl chains (*73*). Neutral DMPC and anionic DMPC/DMPG multilamellar vesicles (MLV) were employed as model membrane systems for eukaryotic and prokaryotic membranes, respectively.

^{31}P NMR of Phospholipid Bilayers. The ^{31}P static NMR spectra for DMPC and DMPC/DMPG MLV exhibited CSAs of −43 and −38 ppm, respectively (Figure 3, Table 2), in agreement with previous studies (*39*, *74*, *75*). The addition of fallaxidin reduced the ^{31}P CSA of DMPC MLV to −38 ppm, and resulted in two contributing powder patterns for DMPC/DMPG MLV. Deconvolution of the two ^{31}P powder patterns using the DMFIT program (*57*) revealed two lipid lamellar component CSAs of −39 (60%) and −34 ppm (40%) (Supporting Information, Figure S4), approximately congruent with the molar fraction of

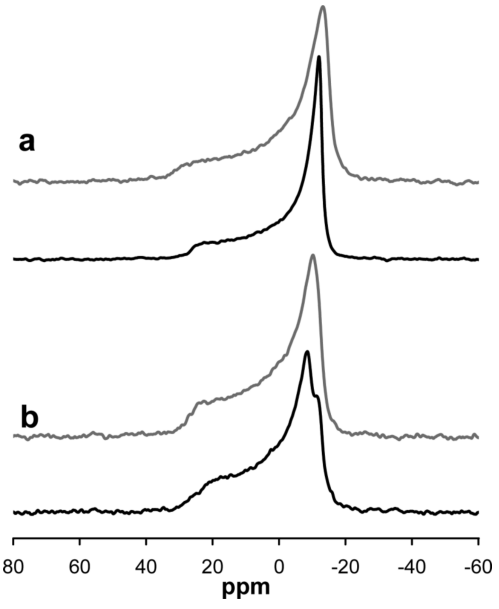

FIGURE 3: ^{31}P NMR spectra obtained for unoriented bilayers of (a) d_{54}-DMPC/DMPC, and (b) d_{54}-DMPC/DMPC/DMPG alone (gray) in the presence of fallaxidin 4.1a (black) at a lipid/peptide ratio of 10:1 at 30 °C.

Table 2: ^{31}P and ^{2}H Spectral Data for DMPC and DMPC/DMPG MLV with the Addition of Fallaxidin 4.1a

			^{2}H quadrupolar coupling constants (kHz)[b,c]			
	^{31}P CSA (ppm)[a]		CD_2		CD_3	
± fallaxidin 4.1a	−	+	−	+	−	+
DMPC MLV	−43	−38	27.6	26.8	3.4	3.5
DMPC/DMPG MLV	−38	−39 (60%)[d] −34 (40%)[d]	27	27.9	3.3	3.4

[a]CSA determined ± 0.5 ppm. [b]Frequency determined ± 0.1 kHz. [c]CD_2 and CD_3 quadrupolar splittings taken from positions 2 and 14 on the deuterated acyl chain of d_{54}-DMPC, respectively. [d]Fitting of the two contributing CSAs was determined using the DMFIT program (*57*).

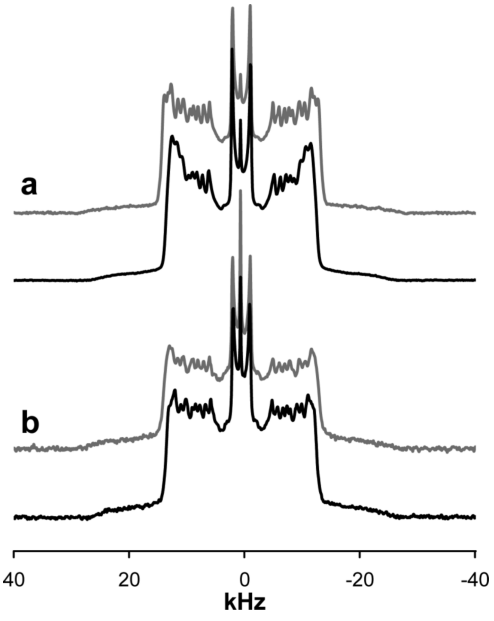

FIGURE 4: ^{2}H NMR spectra obtained for unoriented bilayers of (a) d_{54}-DMPC/DMPC, and (b) d_{54}-DMPC/DMPC/DMPG alone (gray) in the presence of fallaxidin 4.1a (black) at a lipid/peptide ratio of 10:1 at 30 °C.

PC and PG phosphate headgroups, respectively. The decrease in the minor CSA, assigned to the DMPG enriched fraction (*39*), suggests a preferential electrostatic interaction between the cationic peptide and the anionic headgroups of DMPG (*30*, *10*).

^{2}H NMR of Phospholipid Bilayers. The static ^{2}H NMR spectra (Figure 4) were typical for hydrated DMPC and DMPC/DMPG MLV, with a small isotropic peak due to residual D_2O (*40*, *72*, *76*). The ^{2}H NMR spectral powder pattern of the DMPC MLV narrowed upon the addition fallaxidin 4.1a (Figure 4a, Table 2). A small decrease in the S_{CD} order profile (Figure 5) of DMPC MLV was observed at the acyl chain positions 2−6, indicating increased motion or decreased order of the upper part of the chain toward the head of the phospholipid. A small increase in the S_{CD} order was observed at the central region of the acyl chain, which may result from additional steric interactions and reduced space causing a lack of CD_2 mobility as though the presence of the peptide has extended the more ordered "plateau region" further down the acyl chain from positions 8 to 9. Collectively, this effect may result from partial peptide insertion into the bilayer. The ^{2}H NMR spectra of DMPC/DMPG MLV showed a slight increase in quadrupolar splittings upon the addition of fallaxidin 4.1a (Figure 4b), as reflected in the S_{CD} order profile (Figure 5). The peptide appears to order the neutral DMPC in the mixed bilayer.

QCM of Fallaxidin 4.1a on Supported Phospholipid Bilayers. The interaction of fallaxidin 4.1a with DMPC and DMPC/DMPG (2:1) bilayers was investigated using QCM. The frequency change versus time (Δf-t) data for the seventh harmonic are shown in Figure 6. Data obtained on the DMPC bilayer (Figure 6A) revealed initial insertion (decrease in frequency) of fallaxidin 4.1a into the lipid layer for all concentrations. However, at a peptide concentration of 5 μM, membrane disruption was observed. Above this concentration threshold, peptide insertion was followed by lipid removal (increase in frequency).

In contrast, on the DMPC/DMPG (2:1) bilayers (Figure 6B), introduction of fallaxidin 4.1a caused an increase in mass consistent with insertion of the peptide into the bilayer. The harmonics (third, fifth, seventh, and ninth) were uniform up to a threshold mass, after which they diverged (Supporting Information, Figure S6). As observed in our earlier study (*45*), this is consistent with mass addition across the bilayer (i.e., transmembrane) followed by peptide aggregation on the surface of the bilayer. Following a buffer rinse, this surface-bound peptide was removed while leaving some peptide remaining in the bilayer.

In summary, fallaxidin 4.1a disrupted mammalian-like (DMPC) membranes in a concentration-dependent manner. These data are consistent with a two-stage mechanism: insertion followed by a threshold-disruption. Conversely, the interaction of fallaxidin 4.1a with bacterial-like (DMPC/DMPG) membranes, with an increase in mass across the bilayer (Supporting Information, Figure S7b), is consistent with transmembrane peptide insertion, suggesting pore formation (*45*). Transmembrane insertion of peptides has been demonstrated previously by QCM for apidaecins (*44*) using the frequency change over the four harmonics to identify the mechanism of interaction, although in the case of fallaxidin 4.1a, the peptide accumulates on the surface of the membrane following transmembrane saturation.

DISCUSSION

Many of the antimicrobial peptides isolated from amphibians are C-terminally amidated, although an exception is magainin, which carries a free acid (*77*). It has been demonstrated that peptides that have C-terminal amides generally display greater antimicrobial activity (*2*). An increased positive charge usually results in an increase in antimicrobial activity but a large positive charge (e.g., greater than +9) can reduce potency (*78*). This reduction in activity may be a consequence of the higher charge density affecting the propensity of helix formation (*79*).

The solution NMR studies show that the structure of fallaxidin 4.1a is partially helical, yet disrupted about the central region of the peptide. Pro, and to a lesser extent Gly residues, are known to disrupt α-helical structure (*80*, *81*), as is reflected by the observed

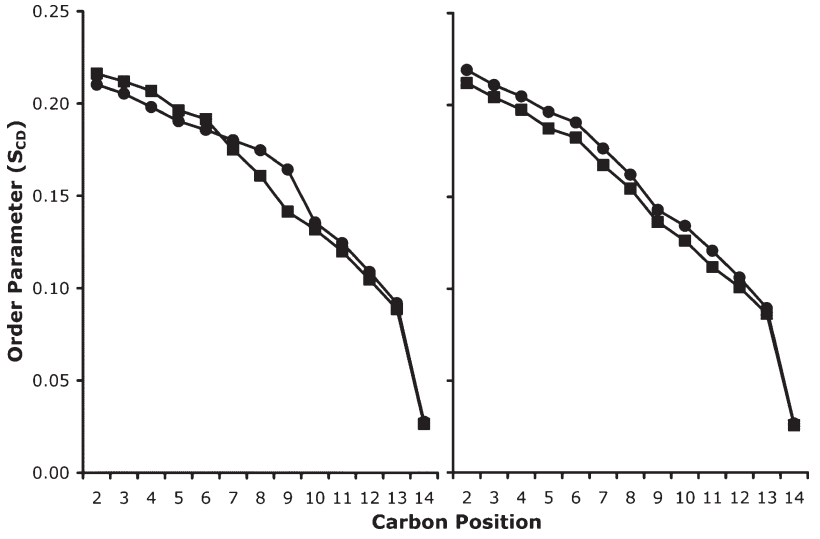

FIGURE 5: Plot of the carbon−deuterium bond order parameters (S_{CD}) against acyl chain carbon position for unoriented bilayers of DMPC-d_{54}/DMPC (left) and DMPC-d_{54}/DMPC/DMPG (right) alone (■) and in the presence of fallaxidin 4.1a (●) at a lipid/peptide ratio of 10:1 at 30 °C.

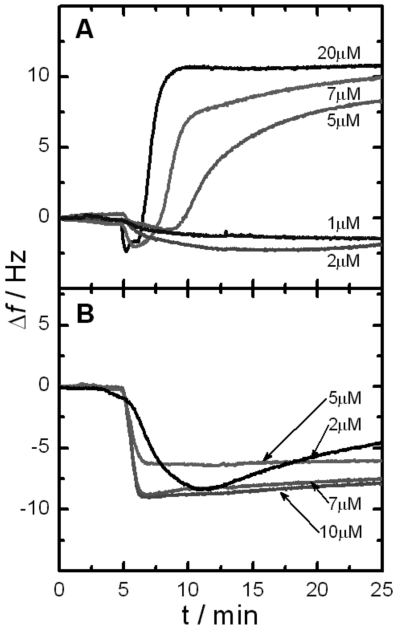

FIGURE 6: QCM traces for the interaction of fallaxidin 4.1a with (A) DMPC, and (B) DMPC/DMPG (2:1) lipid bilayers as a function of peptide concentration (1−20 μM). The frequency change (Δf) versus time is shown. At time = 5 min the peptide was introduced onto the lipid surface and the peptide was incubated for 20 min. The buffer rinse, after ca. 25 min, is not shown.

random coil characteristics about residues from Pro7 toward the C-terminal end of the peptide. However, flexibility of the peptide may enhance interaction with membranes in a similar manner to the central hinge regions of many amphipathic helical peptides (*39*, *82*, *83*). The DPC and DMPC lipids each share the zwitterionic choline headgroup, and DPC micelles mimic a membrane environment by promoting the formation of intramolecular hydrogen bonds in the peptide. Fallaxidin 4.1a could be assumed to adopt a similar structure in the DPC micelles as in DMPC MLVs, though the curvature on the membrane surface of DPC micelles may perturb the propensity of the peptide to form a helical structure. The mixed DMPC/DMPG surface has a net negative surface charge on the membrane. The additional electrostatic interactions with the cationic/polar side chains may induce a more helical secondary structure due to facial alignment of the cationic side chains on one face of a proposed α-helix, as anticipated from an Edmundson helical wheel projection (Supporting Information, Figure S5).

The solid-state NMR and QCM of fallaxidin 4.1a exhibited different interactions with the DMPC and DMPC/DMPG lipid systems. The ^{31}P NMR powder pattern (CSA) of DMPC MLV indicates a significant increase in the mobility and/or change in orientation of the phospholipid headgroups upon addition of fallaxidin 4.1a. Also the S_{CD} order profiles determined from ^{2}H NMR showed an increase in order about the center of the acyl chain (positions 7−9) and a decrease toward the head region of the chain. This difference in the acyl chain order may indicate incorporation of the peptide into the membrane surface (interfacial) region, leading to increased spacing of the lipid headgroups. This would lead to a change in dynamics about the upper region of the acyl chain, as shown by the decreased S_{CD} order parameters and the decrease in the ^{31}P CSA. The insertion and subsequent rapid mass removal upon addition to DMPC supported lipid bilayer at concentrations ≥5 μM observed using QCM suggests the peptide interacts via a surface (carpet) interaction and a possible interfacial insertion.

With the addition of fallaxidin 4.1a to the negatively charged DMPC/DMPG MLV, the contributing ^{31}P CSA of the DMPG enriched component decreased, while the ^{31}P CSA of the DMPC component remained relatively unchanged. A decrease in ^{31}P CSA is typically associated with increased headgroup mobility or an alteration in headgroup conformation away from the bilayer normal (*84*). This suggests an associative electrostatic interaction of the PG head groups with the fallaxidin 4.1a. The deuterium NMR, however, revealed an increase in the acyl chain order of the DMPC phospholipids. Fallaxidin 4.1a may form toroidal pores in the membrane as described for melittin (*85*) and cupiennin (*39*), leading to disordering and a decrease in the ^{31}P CSA of the DMPG enriched lipid fraction and slight ordering of the DMPC enriched lipid fraction. The PG head groups may orient themselves about the lumen of the toroidal pores, as evident in the ^{31}P NMR previously reported by Pukala et al. (*39*). The additional membrane curvature about the toroidal pore would affect the averaging of the ^{31}P shielding tensor relative to a planar membrane surface; hence the observed reduction in

^{31}P CSA. This could result in the decrease in the ^{31}P CSA for the DMPG and an increase in order for the DMPC acyl chains. Supporting the NMR results, the QCM data for fallaxidin 4.1a with DMPC/DMPG (2:1) bilayers showed a transmembrane interaction, consistent with that observed for caerin 1.1 with DMPC/DMPG (4:1) bilayers (*45*). Transmembrane peptide insertion was observed for all peptide concentrations used in this study (1−20 μM). Upon saturation of the bilayer, excess fallaxidin 4.1a bound to the surface of the membrane and these loosely associated peptide aggregates were readily removed by rinsing with buffer solution.

From the antimicrobial activity data, fallaxidin 4.1a appears to be cytolytic toward only the Gram positive bacteria tested, which is similar to many antimicrobial peptides (*14*, *82*), and the amidated N-terminus significantly increased the peptide activity compared to the wild type peptide. The solid-state NMR and QCM results show a differential interaction of fallaxidin 4.1a with neutral DMPC and anionic DMPC/DMPG bilayers, with possible transmembrane insertion in the latter, which mimic the charge of bacterial membranes. The structure of the peptide in micelles indicates that the charged residues of the peptide could interact with the anionic lipid to form pores in membranes and result in the antimicrobial activity of the peptide. The formation of pores at low peptide concentration ($\geq$1 μM) in anionic membranes, combined with the disruption of neutral membranes at higher peptide concentrations ($\geq$5 μM), points to a concentration-dependent cell-selective antimicrobial activity of fallaxidin 4.1a. Further modification of fallaxidin 4.1a could lead to possible development of enhanced selectivity toward Gram positive bacteria.

SUPPORTING INFORMATION AVAILABLE

Tables of NMR chemical shifts, structural statistics, and experimental restraints for fallaxidin 4.1a in DPC micelles, and ^{2}H NMR quadrupolar splittings and S_{CD} order parameters for phospholipid bilayers; plus NMR chemical shifts and spectra, and Ramachandran plot of fallaxidin 4.1a in DPC micelles; ^{31}P NMR spectra for PC/PG bilayers in the presence of fallaxidin 4.1a; helical wheel projections for fallaxidin 4.1a; and QCM traces for the frequency change of fallaxidin 4.1a in phospholipid bilayers. This material is available free of charge via the Internet at http://pubs.acs.org.

REFERENCES

1. Bowan, H. G. (2000) Innate immunity and the normal microflora. *Immunol. Rev. 173*, 5–16.
2. Strandberg, E., Tiltak, D., Ieronimo, M., Kanithasen, M., Wadhwani, P., and Ulrich, A. S. (2007) Influence of C-terminal amidation on the antimicrobial and haemolytic activities of cationic α-helical peptides. *Pure Appl. Chem. 79*, 717–728.
3. Simonetti, O., Cirioni, O., Goteri, G., Ghiselli, R., Kamysz, W., Kamysz, E., Silvestri, C., Orlando, F., Barucca, C., Scalise, A., Saba, V., Scalise, G., Giacometti, A., and Offidani, A. (2008) Temporin A is effective in MRSA-infected wounds through bactericidal activity and acceleration of wound repair in a murine model. *Peptides 29*, 520–528.
4. Livermore, D. (2004) Can better prescribing turn the tide of resistance? *Nat. Rev. Microbiol. 2*, 73–78.
5. Mazel, D., and Davies, J. (1999) Antibiotic resistance in microbes. *Cell. Mol. Life Sci. 56*, 742–754.
6. Bechinger, B. (1997) Structure and functions of channel-forming peptides - magainins, cecropins, melittin and alamethicin. *J. Membr. Biol. 156*, 197–211.
7. Epand, R. M., Shai, Y. C., Segrest, J. P., and Anantharamaiah, G. M. (1995) Mechanisms for the modulation of membrane bilayer properties by amphipathic helical peptides. *Biopolymers 37*, 319–338.
8. Matsuzaki, K., Sugishita, K., and Miyajima, K. (1999) Interactions of an antimicrobial peptide, magainin 2, with lipopolysaccharide-containing liposomes as a model for outer membranes of Gram-negative bacteria. *FEBS Lett. 449*, 221–224.
9. Oren, Z., and Shai, Y. (1998) Mode of action of linear amphipathic α-helical antimicrobial peptides. *Biopolymers 47*, 451–463.
10. Hori, Y., Demura, M., Niidome, T., Aoyagi, H., and Asakura, T. (1999) Orientational behavior of phospholipid membranes with mastoparan studied by 31P solid state NMR. *FEBS Lett. 455*, 228–232.
11. Sitaram, N., and Nagaraj, R. (2002) The therapeutic potential of host-defense antimicrobial peptides. *Curr. Drug Targets 3*, 259–267.
12. Van Compernolle, S. E., Taylor, R. J., Oswald-Richter, K., Jiang, J., Youree, B. E., Bowie, J. H., Tyler, M. J., Conlon, J. M., Wade, D., Aiken, C., Dermody, T. S., KewalRamani, V. N., Rollins-Smith, L. A., and Unutmaz, D. (2005) Antimicrobial peptides from amphibian skin potently inhibit human immunodeficiency virus infection and transfer of virus from dendritic cells to T cells. *J. Virol. 79*, 11598–11606.
13. Barra, D., Simmaco, M., and Boman, H. G. (1998) Gene-encoded peptide antibiotics and innate immunity. Do 'animalcules' have defence budgets? *FEBS Lett. 430*, 130–134.
14. Andreu, D., and Rivas, L. (1998) Animal antimicrobial peptides: An overview. *Biopolymers 47*, 415–433.
15. Pukala, T. L., Bowie, J. H., Maselli, V. M., Musgrave, I. F., and Tyler, M. J. (2006) Host-defence peptides from the glandular secretions of amphibians: Structure and activity. *Nat. Prod. Rep. 23*, 368–393.
16. Shai, Y. (1995) Molecular recognition between membrane-spanning polypeptides. *Trends Biochem. Sci. 20*, 460–464.
17. Shai, Y., and Oren, Z. (2001) From "carpet" mechanism to de-novo designed diastereomeric cell-selective antimicrobial peptides. *Peptides 22*, 1629–1641.
18. Huang, H. W. (2000) Action of antimicrobial peptides: Two-state model. *Biochemistry 39*, 8347–8352.
19. Andreu, D., Ubach, J., Boman, A., Wahlin, B., Wade, D., Merrifield, R. B., and Boman, H. G. (1992) Shortened cecropin A-melittin hybrids - significant size reduction retains potent antibiotic activity. *FEBS Lett. 296*, 190–194.
20. Cornell, B. A., Separovic, F., Baldassi, A. J., and Smith, R. (1988) Conformation and orientation of gramicidin A in oriented phospholipid bilayers measured by solid state carbon-13 NMR. *Biophys. J. 53*, 67–76.
21. Rozek, T., Bowie, J. H., Wallace, J. C., and Tyler, M. J. (2000) The antibiotic and anticancer active aurein peptides from the Australian bell frogs *Litoria aurea* and *Litoria raniformis*. Part 2. Sequence determination using electrospray mass spectrometry. *Rapid Commun. Mass Spectrom. 14*, 2002–2011.
22. Wegener, K. L., Wabnitz, P. A., Carver, J. A., Bowie, J. H., Chia, B. C. S., Wallace, J. C., and Tyler, M. J. (1999) Host defence peptides from the skin glands of the Australian Blue Mountains tree frog *Litoria citropa*. Solution structure of the antibacterial peptide citropin 1.1. *Eur. J. Biochem. 265*, 627–637.
23. Stone, D. J. M., Waugh, R. J., Bowie, J. H., Wallace, J. C., and Tyler, M. J. (1993) Peptides from Australian frogs. The structures of the caerins from *Litoria caerulea*, J. Chem. Res. (S) 138, (M) 910−936.
24. Waugh, R. J., Stone, D. J. M., Bowie, J. H., Wallace, J. C., and Tyler, M. J. (1993) Peptides from Australian frogs. The structures of the caerins and caeridins from *Litoria gilleni*, J. Chem. Res. (S) 139, (M) 937−961.
25. Wegener, K. L., Brinkworth, C. S., Bowie, J. H., Wallace, J. C., and Tyler, M. J. (2001) Bioactive dahlein peptides from the skin secretions of the Australian aquatic frog *Litoria dahlii*: Sequence determination by electrospray mass spectrometry. *Rapid Commun. Mass Spectrom. 15*, 1726–1734.
26. Waugh, R. J., Raftery, M. J., Bowie, J. H., Wallace, J. C., and Tyler, M. J. (1996) The structures of the frenatin peptides from the skin secretions of the giant tree frog, *Litoria infrafrenata*. *J. Pept. Sci. 2*, 117–124.
27. Rozek, T., Waugh, R. J., Steinborner, S. T., Bowie, J. H., Tyler, M. J., and Wallace, J. C. (1998) The maculatin peptides from the skin glands of the tree frog *Litoria genimaculata* - a comparison of the structures and antibacterial activities of maculatin 1.1 and caerin 1.1. *J. Peptide Sci. 4*, 111–115.
28. Brinkworth, C. S., Bowie, J. H., Tyler, M. J., and Wallace, J. C. (2002) A comparison of the host defence skin peptides of the New Guinea tree frog (*Litoria genimaculata*) and the fringed tree frog (*Litoria eucnemis*). The link between the caerin and the maculatin antimicrobial peptides. *Aust. J. Chem. 55*, 605–610.
29. Wong, H., Bowie, J. H., and Carver, J. A. (1997) The solution structure and activity of caerin 1.1, an antimicrobial peptide from

the Australian green tree frog, *Litoria splendida*. *Eur. J. Biochem. 247*, 545–557.
30. Gehman, J. D., Luc, F., Hall, K., Lee, T.-H., Boland, M. P., Pukala, T. L., Bowie, J. H., Aguilar, M.-I., and Separovic, F. (2008) Effect of antimicrobial peptides from Australian tree frogs on anionic phospholipid membranes. *Biochemistry 47*, 8557–8565.
31. Apponyi, M. A., Pukala, T. L., Brinkworth, C. S., Maselli, V. M., Bowie, J. H., Tyler, M. J., Booker, G. W., Wallace, J. C., Carver, J. A., Separovic, F., Doyle, J., and Llewellyn, L. E. (2004) Host-defence peptides of Australian anurans: Structure, mechanism of action and evolutionary significance. *Peptides 25*, 1035–1054.
32. Jackway, R. J., Bowie, J. H., Bilusich, D., Musgrave, I. F., Surinya-Johnson, K. H., Tyler, M. J., and Eichinger, P. C. (2008) The fallaxidin peptides from the skin secretion of the Eastern Dwarf Tree Frog *Litoria fallax*. Sequence determination by positive and negative ion electrospray mass spectrometry: antimicrobial activity and cDNA cloning of the fallaxidins. *Rapid Commun. Mass Spectrom. 22*, 3211–3519.
33. Smet, K., and Contreras, R. (2005) Human antimicrobial peptides: Defensins, cathelicidins and histatins. *Biotechnol. Lett. 27*, 1337–1347.
34. Wang, Z., and Wang, G. (2004) APD: The antimicrobial peptide database. *Nucleic Acids Res. 32*, D590–D592.
35. Bechinger, B. (2005) Detergent-like properties of magainin antibiotic peptides: a 31P solid-state NMR spectroscopy study. *Biochim. Biophys. Acta 1712*, 101–108.
36. Bechinger, B. (1999) The structure, dynamics and orientation of antimicrobial peptides in membranes by multidimensional solid-state NMR spectroscopy. *Biochim. Biophys. Acta 1462*, 157–183.
37. Lu, J., Damodaran, K., Blazyk, J., and Lorigan, G. A. (2005) Solid-state nuclear magnetic resonance relaxation studies of the interaction mechanism of antimicrobial peptides with phospholipid bilayer systems. *Biochemistry 44*, 10208–10217.
38. Spooner, P. J. R., and Watts, A. (1991) Reversible unfolding of cytochrome c upon interaction with cardiolipin bilayers. II. Evidence from phosphorus-31 NMR measurements doi:10.1021/bi00230a011, Biochemistry 30, 3880−3885.
39. Pukala, T. L., Boland, M. P., Gehman, J. D., Kuhn-Nentwig, L., Separovic, F., and Bowie, J. H. (2007) Solution structure and interaction of cupiennin 1a, a spider venom peptide, with phospholipid bilayers. *Biochemistry 46*, 3576–3585.
40. Lu, D., Vavasour, I., and Morrow, M. R. (1995) Smoothed acyl chain orientational order parameter profiles in dimyristoylphosphatidylcholine-distearoylphosphatidylcholine mixtures: a 2H-NMR study. *Biophys. J. 68*, 574–83.
41. Watts, A. (1998) Solid-state NMR approaches for studying the interaction of peptides and proteins with membranes. *Biochim. Biophys. Acta 1376*, 297–318.
42. Tiburu, E. K., Karp, E. S., Birrane, G., Struppe, J. O., Chu, S., Lorigan, G. A., Avraham, S., and Avraham, H. K. (2006) ^{31}P and ^{2}H Relaxation studies of helix vii and the cytoplasmic helix of the human cannabinoid receptors utilizing solid-state NMR techniques. *Biochemistry. 45*, 7356–7365.
43. Mechler, A., Praporski, S., Piantavigna, S., Heaton, S. M., Hall, K. N., Aguilar, M.-I., and Martin, L. L. (2009) Structure and homogeneity of pseudo-physiological phospholipid bilayers and their deposition characteristics on carboxylic acid terminated self-assembled monolayers. *Biomaterials 30*, 682–689.
44. Piantavigna, S., Czihal, P., Mechler, A., Richter, M., Hoffmann, R., and Martin, L. (2009) Cell penetrating apidaecin peptide interactions with biomimetic phospholipid membranes. *Int. J. Pept. Res. Therap. 15*, 139–146.
45. Mechler, A., Praporski, S., Atmuri, K., Boland, M., Separovic, F., and Martin, L. L. (2007) Specific and selective peptide-membrane interactions revealed using quartz crystal microbalance. *Biophys. J. 93*, 3907–3916.
46. Maeji, N. J., Bray, A. M., Valerio, R. M., and Wang, W. (1995) Larger scale multipin peptide synthesis. *J. Pept. Res. 8*, 33–38.
47. Marion, D., and Wüthrich, K. (1983) Application of phase sensitive two-dimensional correlated spectroscopy (COSY) for measurements of ^{1}H-^{1}H spin-spin coupling constants in proteins. *Biochem. Biophys. Res. Commun. 113*, 967–974.
48. Wüthrich, K. (1986) NMR of Proteins and Nucleic Acids , John Wiley and Sons, New York.
49. Xu, R. X., Word, J. M., Davis, D. G., Rink, M. J., Willard, D. H., and Gampe, R. T. (1995) Solution structure of the human pp60$^{c\text{-}src}$ SH2 domain complexed with a phosphorylated tyrosine pentapeptide. *Biochemistry 34*, 2107–2121.
50. Nilges, M., Macias, M. J., Odonoghue, S. I., and Oschkinat, H. (1997) Automated NOESY interpretation with ambiguous distance restraints - the refined NMR solution structure of the pleckstrin homology domain from β-spectrin. *J. Mol. Biol. 269*, 408–422.
51. Linge, J. P., Habeck, M., Rieping, W., and Nilges, M. (2003) ARIA: Automated NOE assignment and NMR structure calculation. *Bioinformatics 19*, 315–316.
52. Folmer, R. H. A., Hilbers, C. W., Konings, R. N. H., and Nilges, M. (1997) Floating stereospecific assignment revisited - application to an 18 kDa protein and comparison with J-coupling data. *J. Biomol. NMR 9*, 245–258.
53. Pari, K., Mueller, G. A., DeRose, E. F., Kirby, T. W., and London, R. E. (2003) Solution structure of the RNase H domain of the HIV-1 reverse transcriptase in the presence of magnesium. *Biochemistry 42*, 639–650.
54. Kang, R. S., Daniels, C. M., Francis, S. A., Shih, S. C., Salerno, W. J., Hicke, L., and Radhakrishnan, I. (2003) Solution structure of a CUE-ubiquitin complex reveals a conserved mode of ubiquitin binding. *Cell 113*, 621–630.
55. Humphrey, W., Dalke, A., and Schulten, K. (1996) VMD - visual molecular dynamics. *J. Mol. Graphics 14*, 33–38.
56. Koradi, R., Billeter, M., and Wüthrich, K. (1996) MOLMOL - a program for display and analysis of macromolecular structures. *J. Mol. Graphics 14*, 51–55.
57. Massiot, D., Fayon, F., Capron, M., King, I., Le Calvé, S., Durand, J.-O., Bujoli, B., Gan, Z., and Hoatson, G. (2002) Modelling one- and two-dimensional solid-state NMR spectra. *Magn. Reson. Chem. 40*, 70–76.
58. Smith, I. C. P., and Ekiel, I. H. (1984) Phosphorus-31 NMR of phospholipids in membranes in *Phosphorus-31 NMR*. Principles and Applications (Garenstein, D. G., Ed.) pp 447−475, Academic Press Inc., London.
59. Davis, J. H., Jeffrey, K. R., Bloom, M., Valic, M. I., and Higgs, T. P. (1976) Quadrupolar echo deuteron magnetic resonance spectroscopy in ordered hydrocarbon chains. *Chem. Phys. Lett. 42*, 390–394.
60. Whittall, K. P., Sternin, E., Bloom, M., and Mackay, A. L. (1989) Time- and frequency-domain "dePakeing" using inverse theory. *J. Magn. Reson. 84*, 64–71.
61. Sternin, E., Bloom, M., and MacKay, A. L. (1983) De-Pake-ing of NMR spectra. *J. Magn. Reson. 55*, 274–282.
62. Galassi, M., Davies, J., Theiler, J., Gough, B., Jungman, G., Booth, M., and Rossi, F. (2008) GNU Scientific Library , 1.11 ed.
63. Williams, T., Kelley, C., Campbell, J., Kotz, D., and Lang, R. (2007) gnuplot, An Interactive Plotting Program , The Free Software Foundation.
64. Jackway, R. J. (2008) Biologically active peptides from Australian amphibians , Ph.D. Thesis, University of Adelaide.
65. Zhou, N. E., Zhu, B., Sykes, B. D., and Hodges, R. S. (1992) Relationship between amide proton chemical shifts and hydrogen bonding in amphipathic α-helical peptides. *J. Am. Chem. Soc. 114*, 4320–4326.
66. Wishart, D. S., Bigam, C. G., Holm, A., Hodges, R. S., and Sykes, B. D. (1995) H-1, C-13 and N-15 random coil NMR chemical shifts of the common amino acids. 1. Investigations of nearest-neighbor effects. *J. Biomol. NMR. 5*, 67–81.
67. Zhou, N. E., Zhu, B. Y., Sykes, B. D., and Hodges, R. S. (2002) Relationship between amide proton chemical shifts and hydrogen bonding in amphipathic α-helical peptides. *J. Am. Chem. Soc. 114*, 4320–4326.
68. Wüthrich, K., Billeter, M., and Braun, W. (1984) Polypeptide secondary structure determination by nuclear magnetic resonance observation of short proton-proton distances. *J. Mol. Biol. 180*, 715–740.
69. Seelig, J. (1978) ^{31}P nuclear magnetic resonance and the head group structure of phospholipids in membranes. *Biochim. Biophys. Acta 515*, 105–140.
70. Davis, J. H. (1983) The description of membrane lipid conformation, order and dynamics by 2H-NMR. *Biochim. Biophys. Acta 737*, 117–171.
71. Boden, N., Jones, S. A., and Sixl, F. (1991) On the use of deuterium nuclear magnetic resonance as a probe of chain packing in lipid bilayers. *Biochemistry 30*, 2146–2155.
72. Lafleur, M., Fine, B., Sternin, E., Cullis, P. R., and Bloom, M. (1989) Smoothed orientational order profile of lipid bilayers by 2H-nuclear magnetic resonance. *Biophys. J. 56*, 1037–41.
73. Fyfe, C. A. (1983) Solid State NMR for Chemists , CFC Press, Ontario.
74. Balla, M. S., Bowie, J. H., and Separovic, F. (2004) Solid-state NMR study of antimicrobial peptides from Australian frogs in phospholipid membranes. *Eur. Biophys. J. 33*, 109–116.
75. Bonev, B., Watts, A., Bokvist, M., and Grobner, G. (2001) Electrostatic peptide-lipid interactions of amyloid-b peptide and pentalysine

with membrane surfaces monitored by ^{31}P MAS NMR. *Phys. Chem. Chem. Phys. 3*, 2904–2910.
76. Otten, D., Brown, M. F., and Beyer, K. (2000) Softening of membrane bilayers by detergents elucidated by deuterium NMR spectroscopy. *J. Phys. Chem. B 104*, 12119–12129.
77. Zasloff, M. (1987) Magainins, a class of antimicrobial peptides from *Xenopus* skin: Isolation, characterization of two active forms, and partial cDNA sequence of a precursor. *Proc. Natl. Acad. Sci. U. S. A. 84*, 5449–5453.
78. Giangaspero, A., Sandri, L., and Tossi, A. (2001) Amphipathic alpha helical antimicrobial peptides. *Eur. J. Biochem. 268*, 5589–5600.
79. Zelezetsky, I., and Tossi, A. (2006) Alpha-helical antimicrobial peptides - using a sequence template to guide structure-activity relationship studies. *Biochim. Biophys. Acta 1758*, 1436–1449.
80. Gunasekaran, K., Nagarajaram, H. A., Ramakrishnan, C., and Balaram, P. (1998) Stereochemical punctuation marks in protein structures: glycine and proline containing helix stop signals. *J. Mol. Biol. 275*, 917–932.
81. Woolfson, D. N., and Williams, D. H. (1990) The influence of proline residues on [alpha]-helical structure. *FEBS Lett. 277*, 185–188.
82. Pukala, T. L., Bowie, J. H., Maselli, V. M., Musgrave, I. F., and Tyler, M. J. (2006) Host-defense peptides from the glandular secretions of amphibians: structure and activity. *Nat. Prod. Rep. 23*, 368–393.
83. Rozek, T., Wegener, K. L., Bowie, J. H., Olver, I. N., Carver, J. A., Wallace, J. C., and Tyler, M. J. (2000) The antibiotic and anticancer active aurein peptides from the Australian bell frogs *Litoria aurea* and *Litoria raniformis*. The solution structure of aurein 1.2. *Eur. J. Biochem. 267*, 5330–5341.
84. Kohler, S. J., and Klein, M. P. (1977) Orientation and dynamics of phospholipid head groups in bilayers and membranes determined from ^{31}P nuclear magnetic resonance chemical shielding tensors. *Biochemistry 16*, 519–526.
85. Yang, L., Harroun, T. A., Weiss, T. M., Ding, L., and Huang, H. W. (2001) Barrel-stave model or toroidal model? A case study on melittin pores. *Biophys. J. 81*, 1475–1485.